

Thermal stability and crystallization of *N*-alkyl-*N*-alkyl'-pyrrolidinium imides

Claudia Simona Stefan · Daniel Lemordant ·
Philippe Biensan · Clémence Siret ·
Bénédicte Claude-Montigny

Received: 24 October 2009 / Accepted: 4 May 2010 / Published online: 28 May 2010
© Akadémiai Kiadó, Budapest, Hungary 2010

Abstract A series of *N*-alkyl-*N*-alkyl'-pyrrolidinium-bis(trifluoromethanesulfonyl) imide (TFSI⁻) room temperature ionic liquids (RTILs) has been investigated by means of thermogravimetric analysis (TG), differential scanning calorimetry, FT-IR spectroscopy, and X-ray diffraction analysis. These compounds exhibit a thermal stability up to 548–573 K. The mass loss starting temperature, T_{ml} , falls in a narrow range of temperatures: 578–594 K. FT-IR spectra, performed before and after 24 h isothermal experiments at 553 and 573 K, have confirmed their great thermal stability. Below the ambient temperature, these compounds exhibit a complex behavior. *N*-methyl-*N*-propyl-pyrrolidinium-TFSI is the sole liquid which crystallizes without forming any amorphous phase even after quenching in liquid nitrogen. Its crystalline phase has a melting point, T_m , of 283 ± 1 K. When the amorphous solid is heated, the *N*-butyl-*N*-ethyl-pyrrolidinium-TFSI presents a glass transition temperature, T_g , at 186 K followed by a cold crystallization, T_{cc} , at 225 K, and a final T_m at 262 K. The *N*-butyl-*N*-methyl-pyrrolidinium-TFSI exhibits a T_g between 186 and 181 K, its cold crystallization leading to two different solid phases. Solid phase I has a melting point $T_{I,m} = 252$ K and phase II, $T_{II,m} = 262$ K. When the amorphous phase is obtained at a cooling rate of 10 K/min, its T_{cc} is 204 K, and a metastable solid phase (III) is obtained which transforms into the phase II at 226 K. However, when the sample is quenched, the amorphous phase transforms

into phase II at $T_{cc} = 217$ K and phase I at 239 K. P₁₅-TFSI exhibits the most complicated pattern as, on cooling, it leads to both a crystallized phase at 237 K and an amorphous phase at 191 K. On heating, after a T_g at 186 K and a T_{cc} at 217 K, two solid–solid phase transitions are observed at 239 K and 270 K, the final T_m being 279 K.

Keywords Room temperature ionic liquids · Flammability · Thermal stability · DSC · TG · Isothermal test

Introduction

For over a decade, an increasing number of studies have been devoted to a new class of green solvents, called Ionic Liquids (ILs). Contrary to the organic solvents that are usually volatile and highly flammable, these new solvents have better respect for the environment, thanks to their low volatility and high boiling points. Room temperature ionic liquids (RTILs) are a subcategory among ILs which are liquid below 373 K. Constituted mainly by organic cations and inorganic anions, these molten salts at room temperature present advantages such as: non-flammability, negligible vapor pressure at room-temperature (or even below), and high chemical and thermal stability.

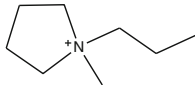
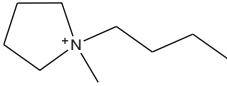
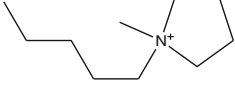
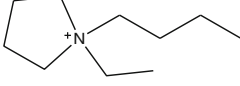
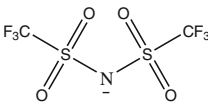
In the past few years, alkyl-pyrrolidinium RTILs have been receiving a great attention. These salts aroused the interests of researchers for many reasons: their good thermal and ionic transport properties [1–10], their large electrochemical window, and their possible applications in electrochemical devices [1, 9–13].

The RTILs investigated here are composed of *N*-alkyl-*N*-alkyl'-pyrrolidinium cation and the bis(trifluoromethanesulfonyl)imide as anion, as reported in Table 1. Even

C. S. Stefan · D. Lemordant · B. Claude-Montigny (✉)
Université François Rabelais, Laboratoire LPCMB (EA 4244),
Equipe CIME, Parc de Grandmont, 37200 Tours, France
e-mail: benedicte.montigny@univ-tours.fr

P. Biensan · C. Siret
SAFT, 111 Bd Alfred Daney, 33074 Bordeaux Cedex, France

Table 1 Names, formula, and abbreviations of *N*-alkyl-*N*-alkyl'-pyrrolidinium imide ($P_{xy}^+TFSI^-$) under consideration

Component	Formula	Abbreviation
<i>N</i> -methyl- <i>N</i> -propyl-pyrrolidinium		P_{13}^+
<i>N</i> -butyl- <i>N</i> -methyl-pyrrolidinium		P_{14}^+
<i>N</i> -methyl- <i>N</i> -pentyl-pyrrolidinium		P_{15}^+
<i>N</i> -butyl- <i>N</i> -ethyl-pyrrolidinium		P_{24}^+
Bis(trifluoromethanesulfonyl)imide		$TFSI^-$

though most of these compounds have been already studied, new insights concerning their thermal behavior are here discussed, and the experimental procedures are revisited.

It is well established that the presence of impurities, even at the trace level, may affect strongly glass transition temperatures (T_g) and that crystallization or melting points can appreciably vary. The purity of RTILs is a key parameter that is able to explain the differences observed in the published results dealing with transport properties, electrochemical, and thermal behaviors [14, 15]. *N*-alkyl-*N*-alkyl'-pyrrolidinium imide RTILs are hydrophobic, owing to the presence of the imide anion $TFSI^-$ [16, 17]. Nevertheless, they are still hygroscopic and may retain moisture: for example, P_{14} - $TFSI^-$ can hold up to 15,000 ppm of water if exposed to a humid atmosphere at ambient temperature [18]. Numerous water molecules remain easily entrapped between the RTIL ions, establishing hydrogen bonds between anions (anion...HOH...anion) [14] or between anions and cations, owing to the amphiphilic nature of water. In general, RTILs are colorless and the fact that the solution is colored is indicative of the presence of an impurity [14, 19, 20], often due to traces of halide intermediaries used for synthesis. Halide impurities have to be removed as far as possible following an adequate purification step [20, 21] prior to performing thermal analysis or any other investigations.

Moreover, the use of different experimental methods for the study of the phase behavior of these complex liquids may lead also to discrepancies among the published results. For this reason, careful attention has been paid to the experimental procedures used for each experiment.

Electrochemical applications such as battery electrolytes require the knowledge of thermal properties, such as the melting points (T_m), the crystallization temperatures (T_c), the glass transition temperatures (T_g), and at elevated temperatures, the mass loss starting temperatures (T_{ml}). The aims of this study are to determine (i) the thermal behavior of P_{xy} - $TFSI^-$ RTILs at temperatures ranging from room temperature to 636 K, (ii) the flammability behavior for security, and (iii) the influence of the experimental method of investigation (scanning and cooling rates) on the phase transition temperatures.

Experimental methods

Materials

All the P_{xy} - $TFSI^-$ ionic liquids (purity >99%) were obtained from Solvionic (Toulouse—France). The halides intermediaries used for the synthesis are reported in Table 2.

Knowing the type and the amount of impurities is important because they may have a great impact in further applications. Residual halides or water entrapped into the RTILs after synthesis are leading to dramatic consequences: it has been reported that residual chloride ranging between 1.5 and 6 wt% increases the viscosity from 30 to 600% [19, 20]. Therefore, we have been working with chloride-free IL (typically <1 ppm of halide). The presence of water can significantly affect the RTIL physicochemical properties such as their viscosity [19] and their electrochemical window [22, 23]. The best way for minimizing the water content in RTIL is to follow the drying method

Table 2 Impurities in *N*-alkyl-*N*-alkyl'-pyrrolidinium imides, halide, and water in the final product

Pyrrolidinium imide	P ₁₃ -TFSI	P ₁₄ -TFSI	P ₁₅ -TFSI	P ₂₄ -TFSI
Halide intermediate used for synthesis	I ⁻	Cl ⁻	Br ⁻	Br ⁻
Halide amount ^a (mg/L)	I ≤ 1	Cl ≤ 1	Br ≤ 1	Br ≤ 1
Water amount ^b (ppm)	1,000	1,230	857	800
Water after drying at 343 K for 72 h (ppm)	86	70	82	66
Water after drying at 393 K for more than 48 h (ppm)	17.4	17.5	16.0	15.8

^a Determined by ionic chromatography

^b Given by the supplier

proposed by Appetecchi et al. [21]: all purchased RTILs were dried in a vacuum oven (SALVIS LAB, Swiss) at 393 K lasting for at least 48 h. The residual water content, checked by Karl-Fischer titration using a KF Coulometer 831 (Metrohm), lies between 15.8 and 17.5 ppm as shown in Table 2. In spite of the optimization of the drying temperature and time, it is not always possible to reduce the water content to a low level. RTILs having hydrophobic anions like TFSI⁻ are easier to dry [18] than those bearing hydrophilic anions like the tetrafluoroborate, BF₄⁻.

After drying, all the RTILs samples were kept under argon atmosphere in a glove box before further analysis.

Methods

Thermal analysis measurements (DSC and TG)

In order to avoid any contamination by water or by the ambient atmosphere, all the samples were prepared under argon in the glove box, and poured into a 50- μ L hermetically sealed aluminum cell. DSC experiments were performed using 10–20 mg (± 0.1 mg) of sample materials. Curves were recorded on a Perkin–Elmer differential scanning calorimeter DSC6 at fixed scanning rates of 2, 5, or 10 K/min, according to the purpose of the experiment. Standard samples of indium (mp 429.7 K) were used for the DSC calibration of temperature measurements over the temperature range of 303–443 K. A dry nitrogen purge was continuously applied into the oven to avoid any water ambient contamination. Experiments above room temperature have been investigated from 298 to 673 K, with the heating and cooling rates of 10 K/min. The oven was cooled by means of cold water. For experiments below room temperature, the DSC 6 apparatus was equipped with a nitrogen gas flow system cooled by means of liquid nitrogen. In order to prevent water condensation, a stream of dry nitrogen was continuously purged over the sample holder. In addition, two different procedures were performed to investigate the stability of phases. The first method consists in cooling the sample from the room

temperature to 153 K (cooling step), stabilization at 153 K for 1 min, and heating up to room temperature (heating step). This method is designed as slow cooling method.

In order to precisely identify the glass transition temperatures (T_g), the crystallization temperatures (T_c), and the melting points (T_m), a scanning rate of 10 K/min was used for all the samples with the exception of P₁₃-TFSI. In order to study the scanning rate influence on melting points and crystallization temperatures, the cooling rate was fixed at 2, 5, and 10 K/min. The second method consists in quenching first the sample in liquid N₂ and then warming it up to room temperature at 10 K/min. Then, a second cycle is operated by cooling down the sample to 153 K at 10 K/min after 1 min of stabilization at room temperature. For P₁₄-TFSI only, a third heating–cooling cycle was performed, to point out the existence of possible metastable phases.

In order to establish the mass loss starting temperature of these RTILs, T_{ml} , the thermal stability of pyrrolidinium ILs was investigated by TG using a Perkin–Elmer TGA7. All the measurements were carried out in an open platinum pan under a dry-argon flow. P₁₃-TFSI, P₁₅-TFSI and P₂₄-TFSI have been studied from 298 to 623 K at a scanning rate of 10 K/min. For the P₁₄-TFSI sample, the temperature range was limited from 298 to 593 K.

FT-IR spectra and long isothermal tests

In order to investigate the RTIL thermal stability over room temperature, P_{xy}-TFSI imides were analyzed by FT-IR spectroscopy before and after a 24-h isothermal step at 553, 573, and 623 K into sealed electrothermal capillary tubes, themselves being introduced into a STUART SMP3 apparatus originally dedicated to melting point measurements. IR spectra were recorded on a Perkin–Elmer spectrum one FT-IR spectrometer.

Flammability tests

In order to investigate the flammability behavior of P_{xy}-TFSI RTILs, tests are performed with strips of Manila

paper soaked with the studied ionic liquid. All the experimental flammability tests were photographed (or recorded) with a digital camera.

X-ray diffraction (XRD)

XRD investigations were performed with an INEL CPS 120 diffractometer using the $\text{CoK}\alpha 1$ radiation (1.7789 Å). Capillaries were sealed into the glove box, to avoid any contamination. Samples were quenched into liquid nitrogen and then heated at 1 K/min with an Oxford system using nitrogen gas vaporized from a cryogenic tank.

Results and discussion

DSC calorimetry, thermogravimetry, and flammability at sub-ambient temperatures

The DSC and TG results obtained for the four *N*-alkyl-*N*-alkyl'-pyrrolidinium imides are reported on the graphs displayed in Fig. 1. The maximal temperature for RTIL use in applications is related to their vapor pressure. Depending on the RTIL nature, decomposition or vaporization may occur when the temperature is raised. In the case of the *N*-alkyl-*N*-alkyl'-pyrrolidinium imides under consideration, the TG curves indicate a mass loss over 573 K. As no large exothermic or endothermic peaks are simultaneously detected on the DSC curves up to, at least, 573 K, it is inferred that only vaporization occurs in the sealed cells. When the cells were open after cooling, no trace of RTIL decomposition was observed. The starting temperatures for mass loss, T_{ml} , in TG experiments are reported in Table 3. Results displayed in Table 3 show that all T_{ml} values fall in a narrow range of temperatures (578–594 K) and are practically independent of the *N*-alkyl chain length. These results are in fairly good agreement with those published in the literature [9, 24, 25]. In addition, the samples placed in sealed capillaries have been submitted to isothermal experiments at 553, 573, and 623 K during 24 h. The visual observation of the samples does not allow us to detect any trace decomposition at the exception of the sample maintained at 623 K for which pyrolysis occurs. In this case, it was unfortunately impossible to analyze the resulting products. In order to confirm that no decomposition phenomenon occurs up to 573 K, FT-IR spectra of the corresponding samples have been performed. As seen on the graphs reported in Fig. 2, no significant change can be noticed among the dry (<20 ppm) (2a), the wet sample (saturated) (2b), and the heated sample (573 K) (2c) P_{15} -TFSI samples. Three peaks correspond to water in these samples at 3,639, 3,564, and 1,622 cm^{-1} : those are clearly visible when spectra 2a and 2b are compared. All

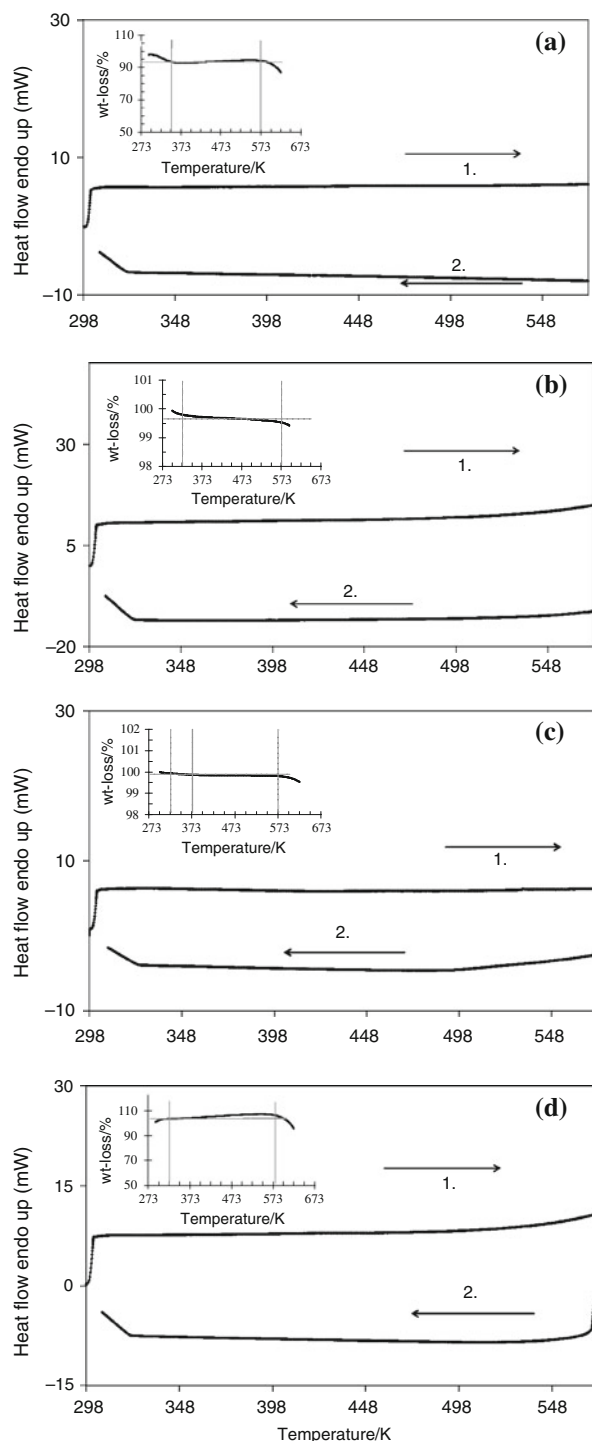
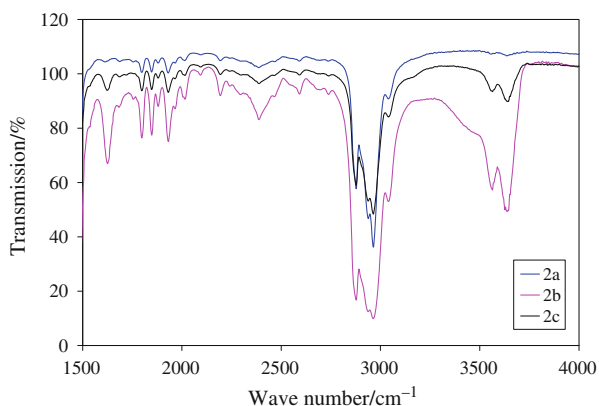


Fig. 1 DSC curves and TG (insert) analysis for P_{13} -TFSI (a), P_{14} -TFSI (b), P_{15} -TFSI (c), and P_{24} -TFSI (d)

these peaks have increased in intensity when the dry sample has been heated at 573 K. It is not clear whether the presence of water in the heated sample comes from the capillary tube or humidity adsorbed during the transfer of the sample from the glove box to the capillary, but, in any

Table 3 P_{xy}-TFSI RTIL mass loss starting temperatures, T_{ml} , from TG analysis

P _{xy} -TFSI	P ₁₃ -TFSI	P ₁₄ -TFSI	P ₁₅ -TFSI	P ₂₄ -TFSI
T_{ml}/K	594 ± 2	578 ± 2	583 ± 2	588 ± 2

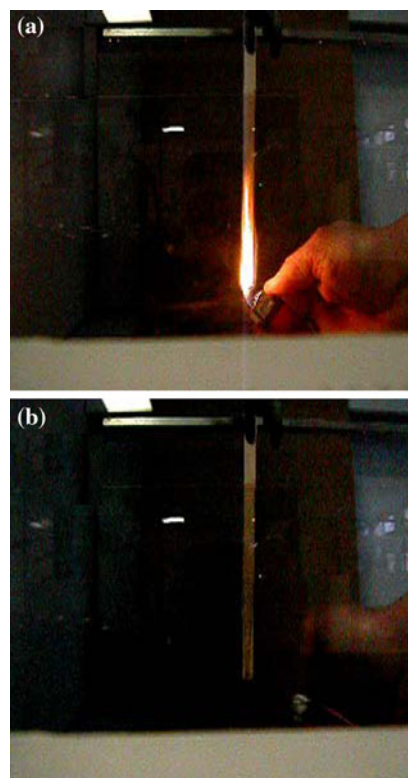
**Fig. 2** FT-IR spectra of P₁₅-TFSI: dry sample (**2a**), water saturated sample (**2b**), and after a 24-h isothermal experiment at 673 K (**2c**)

case, no decomposition occurs. In conclusion, if no other decomposition pathways occurring at lower temperature are accessible [26], then pyrolysis occurs at temperatures over 573 K which restricts the use of these RTILs only at very elevated temperatures. Nevertheless, protic IL exhibit lower decomposition temperatures, as decomposition occurs through shifts in the proton transfer equilibrium between salt form and parent acid/base pairs [23].

For applications, like electrolytes in high temperature batteries or supercapacitors, the thermal stability and the flammability of the electrolyte components are very important. Flammability tests performed for this reason show that it is almost impossible to fire up with a lighter strips of Manila paper soaked with RTILs. As seen in Fig. 3a, the paper soaked in P₁₃-TFSI is first ignited with a gas lighter. After a few seconds, the lighter is removed, and the flame spontaneously extinguishes as seen in Fig. 3b. These results show that, as expected, these RTILs exhibit a very good resisting behavior to flame.

Phase stability under ambient temperature

The influence of the scanning rate and the cooling method has been first investigated using P₁₃-TFSI. DSC experiments have been performed using different scanning rates for the cooling and heating steps, and, for the first cooling step, the samples have been either quenched in liquid N₂ or slowly cooled at 10 K/min down to 153 K. Curves are displayed in Fig. 4a and b, and results are depicted in Table 4. Using the slow cooling method, the curves

**Fig. 3** Flammability test (**a**) lighter flame in contact with the paper soaked with P₁₄-TFSI and **b** flame self-extinguished

(Fig. 4a) and the results displayed in Table 4 show that the freezing temperature of the liquid phase depends on the scanning rate: $T_c = 259, 261,$ and 262 K, respectively at 2, 5, and 10 K/min. This is clearly linked to a supercooling phenomenon as the melting point, $T_m = 283 \pm 1$ K, is higher than the freezing point by about 20 K. The entropy of melting has been calculated from the enthalpy of melting which corresponds to the area under the peak. DSC results obtained for P₁₃-TFSI, using the slow cooling method (10 K/min) and the quenching method are compared in Fig. 4b. Both curves have been run at 10 K/min after the first cooling cycle. On completion of the first heating cycle, the melting temperature is the same, $T_m = 284$ K, and in accordance with the results of Jin et al. [27], no glass transition temperature is detected. Nevertheless, surprisingly MacFarlane et al. [1] have reported a T_g using the quenching method. The crystallization temperatures on the subsequent cooling cycle are slightly different: 265 K (quenching) or 262 K (slow cooling). The main discrepancy between the present results and those of MacFarlane et al. [1] is the formation of an amorphous phase during the quenching step, which is followed by a cold crystallization at 206 K, an exothermic solid–solid phase transition (phase III \rightarrow II at 228 K), an endothermic solid–solid phase transition (phase II \rightarrow I at 255 K), and

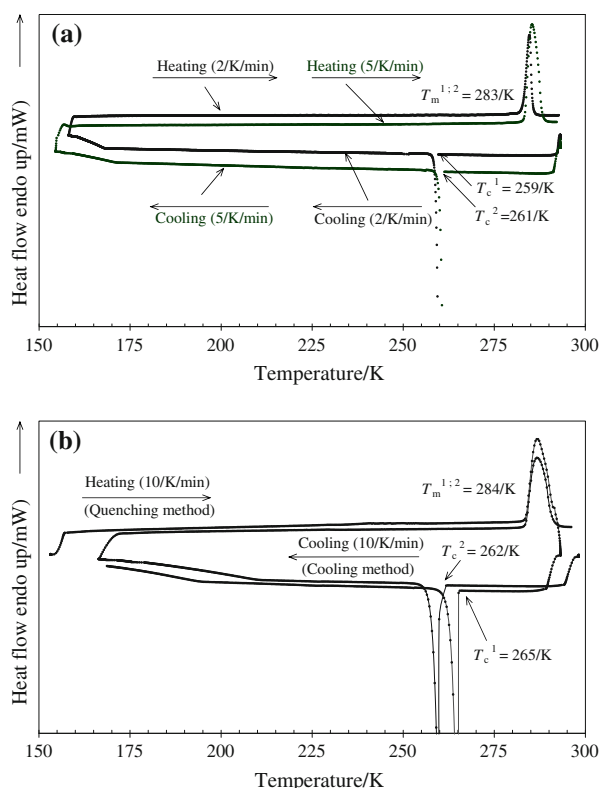


Fig. 4 DSC curves for P₁₃-TFSI, influence of the scanning rate **a** 2 and 5 K/min cooling or heating and **b** 10 K/min heating after cooling at 10 K/min in or quenching

finally a melting point at 285 K. This melting point shows that the crystallized P₁₃-TFSI that we get during the first cooling cycle (slow or quenched) is identical to phase I described by MacFarlane. Similar to Jin et al. [27], we do not observe any amorphous phase followed by solid–solid phase transitions, but only the crystallization of one solid compound (phase I); it seems strange that identical procedures do not lead to the same thermal behavior unless impurities were present in relatively larger amount in MacFarlane samples.

Curves obtained for P₁₅-TFSI are reported in Fig. 5. A cooling rate of 10 K/min was applied between room temperature and 193 K and a slower rate (2 K/min) between 193 and 153 K. Corresponding results are presented in Table 5. During the cooling step, a crystallization occurs at 237 K, followed by a glass transition at $T_g = 191$ K. On the subsequent heating step, T_g is obtained at a slightly lower temperature (186 K). When the temperature is raised over T_g , three exothermic phenomena appear successively at 217, 239 K, and at 270 K. They can be attributed successively to a cold crystallization at $T_{cc} = 217$ K, and two solid–solid phase transitions at $T_{ss,1} = 239$ K and $T_{ss,2} = 270$ K. We may also remark that the sum of the entropies (crystallization + solid–solid phase transitions) $\Sigma\Delta_m S = -44$ J K⁻¹ mol⁻¹ matches well the entropy of

Table 4 DSC analysis of P₁₃-TFSI, influence of the scanning heating rate on the cold crystallization and melting temperatures, and on the entropy of melting (slow cooling method)

Scanning rate/ K/min	T_{cc} /K/min	T_m /K/min	$\Delta_m S$ /J K ⁻¹ mol ⁻¹ (±6%)
2	259	283	61
5	261	283	52
10	262	284	51

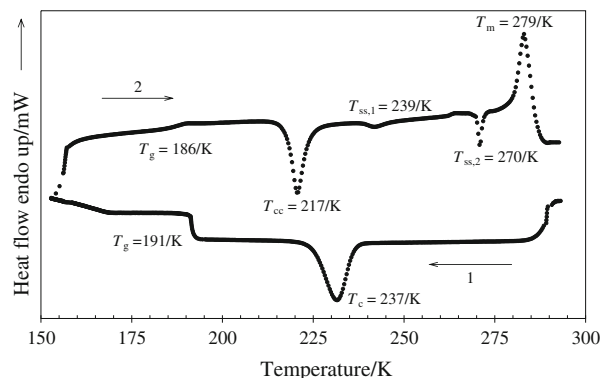


Fig. 5 DSC curve for P₁₅-TFSI when the sample is cooled and heated at 10 K/min

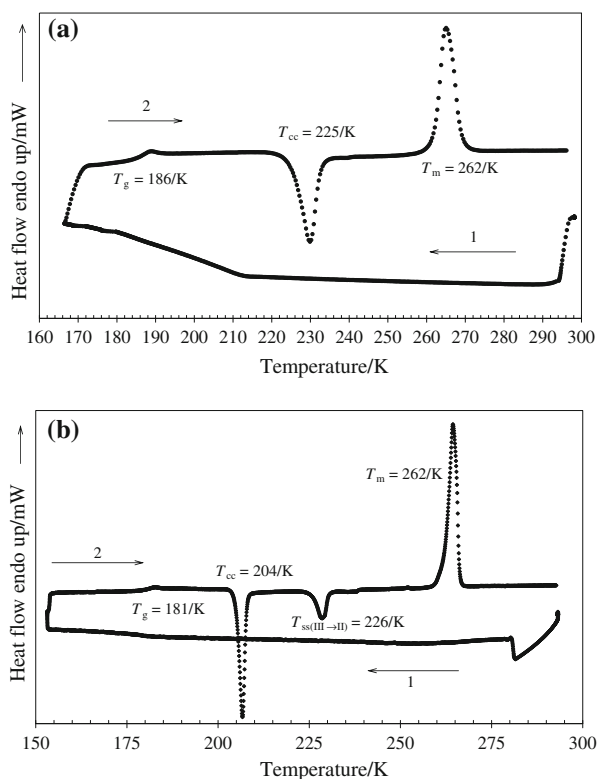
melting that is equal to $\Delta_m S = 46$ J K⁻¹ mol⁻¹. This shows that more ordered crystalline phases are obtained when heating. T_g and T_m values reported in Table 5, are in good agreement with the results of MacFarlane et al. [2], but the entropies of melting are quite different.

Results obtained for P₂₄-TFSI and P₁₄-TFSI are displayed in Fig. 6 and Table 6. Using the slow cooling method, no thermal phenomenon occurs during the cooling step. On the subsequent heating cycle, different phase transitions are observed for both compounds: a glass transition temperature, a cold crystallization followed (P₁₄-TFSI) or not (P₂₄-TFSI) by a solid–solid phase transition, and finally a melting point. T_g are 186 K for P₂₄-TFSI and 181 K for P₁₄-TFSI. The cold crystallization occurs at $T_{cc} = 225$ K for P₂₄-TFSI and $T_{cc} = 204$ K for P₁₄-TFSI, which is followed by an exothermic solid–solid phase transition at 226 K. The crystalline phases are melting at 262 K in both cases. Excepting for T_g values, the ethyl chain in P₂₄-TFSI does not much affect the thermal behavior with respect to P₁₄-TFSI. This suggests that the solid phases obtained at 226 K for P₁₄-TFSI and 225 K for P₂₄-TFSI are identical and that the cold crystallization of P₁₄-TFSI at 204 K leads to a metastable phase which transforms into a stable crystalline phase at 226 K. If we compare these results with those obtained by Fernicola et al. [10] for P₂₄-TFSI, then we can notice that if T_{cc} values are very close together as those authors have reported: $T_{cc} = 228$ K at a scanning rate of 5 K/min, T_m

Table 5 DSC analysis of P₁₅-TFSI, phase transition temperatures and entropy of melting according to the method used for cooling the sample

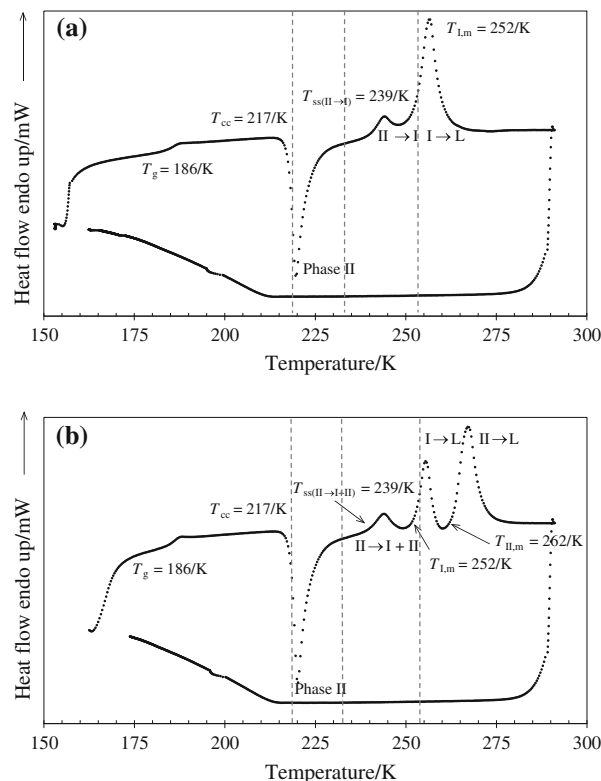
	T_c/K (± 2 K)	T_g/K (± 2 K)	T_{cc}/K (± 2 K)	$T_{ss,1}/K$ (± 2 K)	$T_{ss,2}/K$ (± 2 K)	T_m/K (± 2 K)	$\Delta_m S/J K^{-1} mol^{-1}$ ($\pm 6\%$)
Cooling step ^a	237	191	ND	ND	ND	(–)	(–)
Heating step ^a	ND	186	217	239	270	279	46
Heating step ^a after quenching [2]		190			277	281	80

ND not detected

^a At 10 K/min**Fig. 6** DSC curves for P₂₄-TFSI (a) and P₁₄-TFSI (b) when the sample is cooled and heated at 10 K/min

values differ by 3 K, as they have reported $T_m = 265$ K, but this small difference can be attributed to experimental errors.

The quenching method was also applied to P₁₄-TFSI. After quenching, two heating–cooling cycles were performed. Curves, obtained for P₁₄-TFSI at a scanning

**Fig. 7** DSC curve for a quenched P₁₄-TFSI sample heated and cooled successively at 10 K/min: a first heating–cooling cycle, and b second heating–cooling cycle

rate of 10 K/min are displayed in Fig. 7a for the first heating–cooling cycle and Fig. 7b for the second cycle. Results obtained by analysis of the curves and literature data are listed in Table 7. After quenching, on the first heating step (Fig. 7a) starting from 153 K, a glass

Table 6 DSC analysis of P₂₄-TFSI and P₁₄-TFSI, phase transition temperatures and entropy of melting when the sample is cooled at 10 K/min

	Scanning direction	T_g/K (± 2 K)	T_{cc}/K (± 2 K)	$T_{ss(III-II)}/K$ (± 2 K)	T_m/K (± 2 K)	$\Delta_m S/J K^{-1} mol^{-1}$ ($\pm 6\%$)
P ₂₄ -TFSI	Cooling step	ND	ND	(–)	(–)	(–)
	Heating step	186	225	(–)	262	33.3
P ₁₄ -TFSI	Cooling step	ND	ND	ND	(–)	(–)
	Heating step	181	204	226	262	76.5

ND not detected

Table 7 DSC analysis P₁₄-TFSI phase transition temperatures after quenching the sample

P ₁₄ -TFSI	T_g/K^a	T_{cc}/K^a	$T_{ss(II \rightarrow I)}/K^a$	$T_{ss(II \rightarrow I+II)}/K^a$	$T_{I,m}/K^a$	$T_{II,m}/K^a$
Literature [19]	186	223	249	ND	255	ND
This study (first cycle)	186	217	239	ND	252	ND
This study (second cycle)	186	217	ND	240	252	262

ND not detected

^a Temperature accuracy is ± 2 K

transition temperature is first observed at $T_g = 186$ K (instead of 181 K by slow cooling) followed by a cold crystallization at $T_{cc} = 217$ K (instead of 204 K, slow cooling). When the temperature is raised, a solid–solid endothermic phase transition occurs (II \rightarrow I) at $T_{ss(II \rightarrow I)} = 239$ K, followed by the fusion peak at $T_{I,m} = 252$ K. At the second cycle, the glass transition temperature T_g , cold crystallization T_{cc} , solid–solid transition temperature $T_{ss(II \rightarrow I)}$, and melting temperature $T_{I,m}$ are the same at the second cycle within ± 1 K, but a new endothermic peak appears at 262 K, which is the same as the melting peak obtained by the slow cooling method. On cooling, in both cycles, the liquid phase exhibits a very large supercooling range of temperatures without any detectable DSC signal.

The solid phase melting at 262 K (quoted as phase II) is obtained either by a solid–solid transition III (metastable phase) \rightarrow II at 226 K using the slow cooling method (see Fig. 6b), or by cold crystallization of the quenched sample at 217 K (see Fig. 7b). Solid phase I is characterized by a melting point at 252 K (our results) and is obtained by a solid–solid transition II \rightarrow I occurring at 240 K (± 1 K) after quenching.

In order to investigate the exact nature of the observed solid–solid transitions, a detailed X-ray diffraction study has been run, under same quenching conditions. The X-ray diffraction diagrams obtained at 218, 233, and 253 K are presented in Fig. 8a and b. In Fig. 8a is reported the X-ray diagrams of phase II at 218 and 233 K: the peaks are overlapping indicating that the same crystalline phase is present at these two temperatures. In Fig. 8b is reported the diagram obtained at 253 K: the number of peaks differs from the preceding diagram, but the comparison between diagrams at 218 K (or 233 K) and 253 K indicates that at 253 K, phase II is mixed with another phase that is phase I. This result supports the co-existence of phases I and II above 240 K (at the second cycle) as shown in Fig. 7b. As a consequence, two separate melting points are found: $T_{I,m} = 252$ K for phase I and $T_{II,m} = 262$ K for phase II.

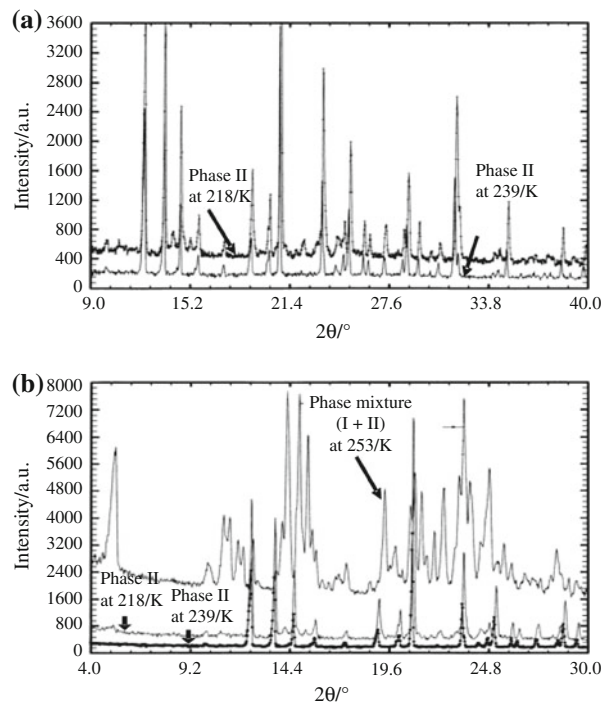


Fig. 8 X-ray diffraction analysis of P₁₄-TFSI at various temperatures after quenching, **a** phase II at 218 and 233 K; **b** phase II at 218 and 233 K, and phase mixture (I + II) at 253 K

Conclusions

The thermal stability of a series of *N*-alkyl-*N*-alkyl'-pyrrolidinium-bis(trifluoromethanesulfonyl)imide RTILs has been investigated. ATG and DSC studies reveal that no RTIL decomposition or vaporization occur below 578 K and as expected, these RTILs exhibit a very good resisting behavior to flame. When the temperature is decreased below ambient temperature, DSC experimental results indicate that phase transition are slightly dependent on the scanning rate, but highly influenced by the cooling method used to obtain the solid phase: quenching or slow cooling. Depending on the method used for cooling, stable or

metastable crystal phases are observed which were identified by means of X-ray diffraction analysis. Comparison with the published results shows that the differences in phase transition temperatures are not only related to experimental errors, but also to the presence of impurities like water and halides whose amounts are often lacking in the literature data.

The thermal stability of the P_{xy}-TFSI RTIL is a great advantage over other RTILs for potential use as electrolytes in high temperature electrochemical devices. Nevertheless, other physical–chemical properties such as ionic transport and electrochemical stability must be considered.

Acknowledgements The authors thank Dr. H. Allouchi (L.P.C.M.B., Université François Rabelais de Tours, France) for the XRD measurements, Drs. E. Colnay (LACCO, Université de Poitiers, France) and A. L. Daltin (D.T.I., Université de Reims Champagne Ardennes, France) for TG measurements.

References

- MacFarlane DR, Meakin P, Sun J, Amini N, Forsyth M. Pyrrolidinium imides: a new family of molten salts and conductive plastic crystal phases. *J Phys Chem B*. 1999;103:4164–70.
- MacFarlane DR, Meakin P, Amini N, Forsyth M. Pyrrolidinium imides: a new family of molten salts and conductive plastic crystal phases. *J Phys Condens Matter*. 2001;13:8257–67.
- MacFarlane DR, Forsyth M. Plastic crystal electrolyte materials: new perspectives on solid state ionics. *Adv Mater*. 2001;12–13:957–66.
- Hill AJ, Huang J, Efthimiadis J, Meakin P, Forsyth M, MacFarlane DR. Microstructural and molecular level characterisation of plastic crystal phases of pyrrolidinium trifluoromethanesulfonyl salts. *Solid State Ionics*. 2002;154–155:119–24.
- Sun J, MacFarlane DR, Forsyth M. Conductive plastic crystal phases of the 1-alkyl-2-methyl pyrrolinium TFSA salts. *Solid State Ionics*. 2002;148:145–51.
- Sun J, MacFarlane DR, Forsyth M. A new family of ionic liquids based on the 1-alkyl-2-methyl pyrrolinium cation. *Electrochim Acta*. 2003;48:1707–11.
- Henderson WA, Passerini S. Phase behavior of ionic liquid–LiX mixtures: pyrrolidinium cations and TFSI[−] anions. *Chem Mater*. 2004;16:2881–5.
- Adebahr J, Ciccossillo N, Shekibi Y, MacFarlane DR, Hill AJ, Forsyth M. The “filler-effect” in organic ionic plastic crystals. Enhanced conductivity by the addition of nano-sized TiO₂. *Solid State Ionics*. 2006;177:827–31.
- Salminen J, Papaiconomou N, Kumar RA, Lee J-M, Kerr J, Newman J, Prausnitz JM. Physicochemical properties and toxicities of hydrophobic piperidinium and pyrrolidinium ionic liquids. *Fluid Phase Equilib*. 2007;261:421–6.
- Fernicola A, Croce F, Scrosati B, Watanabe T, Ohno H. LiTFSI-BEPyTFSI as an improved ionic liquid electrolyte for rechargeable lithium batteries. *J Power Sources*. 2007;174:342–8.
- Sakaebe H, Matsumoto H. *N*-methyl-*N*-propylpiperidinium bis(trifluoromethanesulfonyl)imide (PP₁₃-TFSI)—novel electrolyte base for Li battery. *Electrochem Commun*. 2003;5:594–8.
- Hollenkamp AF, Howlett PC, MacFarlane DR, Forsyth SA (2004) Pyrrolidinium based room temperature ionic liquids as electrolyte in energy storage devices. *PCT Int Appl* 2004; 55 pp. WO 2004082059 A1; Patent 2004.
- Howlett PC, MacFarlane DR, Hollenkamp AF. High lithium metal cycling efficiency in a room-temperature ionic liquid. *Electrochem Solid-State Lett*. 2004;7:A97–101.
- Billard I, Moutiers G, Labet A, El Azzi A, Gaillard G, Mariet C, Lutzenkirchen S. Stability of divalent europium in an ionic liquid: spectroscopic investigations in 1-methyl-3-butylimidazolium hexafluorophosphate. *Inorg Chem*. 2003;42:1726–33.
- Zhang S, Sun N, He X, Lu X, Zhang X. Physical properties of ionic liquids: database and evaluation. *J Phys Chem Ref Data*. 2006;35:1475–517.
- Cammarata L, Kazarian SG, Salter PA, Welton T. Molecular states of water in room temperature ionic liquids. *J Phys Chem Chem Phys*. 2001;3:5192–200.
- Olivier-Bourbigou H, Magna L. Ionic liquids: perspectives for organic and catalytic reactions. *J Mol Catal A*. 2002;182–183:419–37.
- Pitner W. Ionic liquids. Properties and applications. Merck KGaA, Darmstadt, Germany. <http://www.merck.de/servlet/PB/menu>. Accessed June 2008.
- Seddon KR, Stark A, Torres M-J. Influence of chloride, water, and organic solvents on the physical properties of ionic liquids. *Pure Appl Chem*. 2000;72:2275–87.
- Wasserscheid P, Welton T, editors. *Ionic liquids in synthesis*. 2nd ed. Weinheim: Wiley-VCH; 2008.
- Appetecchi GB, Scaccia S, Tizzani C, Alessandrini F, Passerini S. Synthesis of hydrophobic ionic liquids for electrochemical applications. *J Electrochem Soc*. 2006;153:A1685–91.
- Wakizaka Y, Owen J R. Effects of impurities and additives on the stability window of an ionic liquid. *IMLB 2006 June 18-23 Biarritz France*: 2006; abstract #435.
- Zhou Z-B, Matsumoto H, Tatsumi K. Low-melting, low-viscous, hydrophobic ionic liquids: aliphatic quaternary ammonium salts with perfluoroalkyltrifluoroborates. *Chem Eur J*. 2005;11:752–66.
- Pringle JM, Golding J, Baranyai K, Forsyth CM, Deacon GB, Scott JL, MacFarlane DR. The effect of anion fluorination in ionic liquids-physical properties of a range of bis(methanesulfonyl)amide salts. *New J Chem*. 2003;27:1504–10.
- Jagadeeswara Rao Ch, Venkata Krishnan R, Venkatesan KA, Nagarajan K, Srinivasan TG. Thermochemical properties of some bis(trifluoromethyl-sulfonyl)imide based room temperature ionic liquids. *J Therm Anal Calorim*. 2009;97:937–43.
- Hussey CL. Room temperature haloaluminate ionic liquids. Novel solvents for transition metal solution chemistry. *Pure Appl Chem*. 1988;60:1672–763.
- Jin H, O'Hare B, Dong J, Arzhantsev S, Baker GA, Wishart JF, Benesi AJ, Maroncelli M. Physical properties of ionic liquids consisting of the 1-butyl-3-methylimidazolium cation with various anions and the bis(trifluoromethylsulfonyl)imide anion with various cations. *J Phys Chem B*. 2008;112:81–92.